Electrostatic/magnetic ion acceleration through a slowly diverging magnetic nozzle between a ring anode and an on-axis hollow cathode

Cite as: AIP Advances **7**, 065204 (2017); https://doi.org/10.1063/1.4985380
Submitted: 20 March 2017 . Accepted: 26 May 2017 . Published Online: 05 June 2017

A. Sasoh, K. Mizutani, and A. Iwakawa

Electrostatic/magnetic ion acceleration through a slowly diverging magnetic nozzle between a ring anode and an on-axis hollow cathode

A. Sasoh,[a] K. Mizutani, and A. Iwakawa
Department of Aerospace Engineering, Nagoya University, Nagoya 464-8603, Japan

(Received 20 March 2017; accepted 26 May 2017; published online 5 June 2017)

Ion acceleration through a slowly diverging magnetic nozzle between a ring anode and a hollow cathode set on the axis of symmetry has been realized. Xenon was supplied as the propellant gas from an annular slit along the inner surface of the ring anode so that it was ionized near the anode, and the applied electric potential was efficiently transformed to an ion kinetic energy. As an electrostatic thruster, within the examined operation conditions, the thrust, F, almost scaled with the propellant mass flow rate; the discharge current, J_d, increased with the discharge voltage, V_d. An important characteristic was that the thrust also exhibited electromagnetic acceleration performance, i.e., the so-called "swirl acceleration," in which $F \cong J_d B R_a / \sqrt{2}$, where B and R_a were a magnetic field and an anode inner radius, respectively. Such a unique thruster performance combining both electrostatic and electromagnetic accelerations is expected to be useful as another option for in-space electric propulsion in its broad functional diversity. [http://dx.doi.org/10.1063/1.4985380]

Electric in-space propulsion technology, which hereafter will be referred to as just "electric propulsion (EP)," has experienced significant advances in recent years. As a result, its function has been expanded even to the development of "all electric satellites" such as the ABS-3A and EUTELSAT 115 WEST B with the Boeing 702 SP bus system, in which primary propulsion from a geostationary transfer orbit (GTO) is done using only EP. Among existing thrusters, ion thrusters[1] exhibit the highest thrust efficiency, η, and a high specific impulse that is higher than 2000 s. However, owing to the space charge limitation, their thrust density cannot be increased to 10^4 N/m^2. Hall thrusters[1,2] are capable of even higher thrust densities of the order of 10^5 N/m^2 because the ions are accelerated in a quasi-neutral region, where the electrons move in a closed drift motion, yielding a Hall current. The power level and thrust efficiency of Hall thrusters are still undergoing improvements. However, to apply EP to various space missions, diversity in thruster performance, such as thrust, energy conversion efficiency, specific impulse, thrust/power ratio, thrust/weight ratio, and lifetime, should be further improved and extended. A stationary plasma thruster (SPT), a type of Hall thruster, can be accompanied by serious wall erosion, as its insulator wall is exposed in an annular acceleration channel.[1] Mikellides et al.[3] proposed the concept of "magnetic shielding" to alleviate this problem. Ratses et al.[4] developed another type of Hall thruster, the "cylindrical Hall thruster," in which an electric field in the ion acceleration region has radially inward and axial components, to decrease the rate of ion collisions against the insulator walls. However, the electrical potential distribution near the anode was similar to that of SPT, in which the normal vector to the anode surface and the magnetic field are set in the axial and radial directions, respectively. End-Hall ion source has a similar configuration to Hall thruster,[5,6] but is optimized for plasma processing of lower ion energies and larger beam divergence.

[a]Author to whom correspondence should be addressed. Electronic mail: sasoh@nuae.nagoya-u.ac.jp.

Harada et al.[7] proposed the helicon electrostatic thruster (HEST), an electrostatic thruster in which ions produced using a helicon plasma source were accelerated between the inner surface of a ring anode and a cathode placed near the cusp of an applied magnetic field. On the inner surface of the ring anode, a magnetic field has a dominant component in the axial direction. From the anode, a radially inward electric field is generated towards the axis; the ions are accelerated radially inward and then in the axial direction, thereby creating an ion beam energy that is almost equivalent to the discharge voltage.[8] Ichihara et al.[9] developed the diverging magnetic field electrostatic thruster (DM-EST) by utilizing the same electrode and magnetic field configurations as in the HEST, but without the helicon plasma source. By injecting the propellant, argon, only along the inner surface of the ring anode, the ionization near the anode was enhanced, thereby converting almost all the electric potential between the electrodes into ion kinetic energy. Probe measurements confirmed that on the axis near the cusp there existed a field free region where the space potential was almost equal to that at the cathode. This inspired us for a different configuration; a similar potential distribution can be obtained by placing a cathode even on the axis; in that case, a cusp field such as the one in the HEST and DM-EST is not necessary. A slowly diverging magnetic field produced by a solenoid coil should suffice.

In this study, an electrostatic thruster with a ring anode near a propellant injection slit and a cathode that is coaxially set in a slowly diverging magnetic field generated by a solenoid coil is developed, and its thrust characteristics are examined.

Figure 1 schematically illustrates the cross-section of the proposed thruster, which is named the central-cathode, electrostatic thruster (CC-EST). Essentially, the thruster has an axisymmetric configuration. The ring anode is placed in a ceramic cylindrical insulator (Photoveel, Ferrotec co.). The inner radius of the ring anode, R_a, equals either 29 mm or 40 mm (Fig. 1). The outer radius of the anode is 43.8 mm, and the anode loosely fits into the cylindrical insulator. The ring anode and the central ceramic cylinder made of alumina are coaxially set with a clearance of width 1.5 mm that acts as an annular slit; the former extrudes beyond the latter by 8 mm. Through this slit, the propellant gas is injected toward the acceleration region with a mass flow rate of $\dot{m}_a$. The hollow cathode is set in the alumina cylinder on the center axis. Its keeper tip is flush mounted on the end surface of the alumina cylinder. The cathode tip is a commercial product (Kaufmann & Robinson Inc., LHC-03-AE1-01, 20 A maximum). Through the cathode tip, a cathode working gas, xenon (99.995%), is fed at a mass flow rate of $\dot{m}_c$. A keeper current is kept to 2A. The keeper potential to the cathode tip which depended on operation conditions varied from 15 to 25 V. A slowly diverging magnetic field is applied using a solenoid coil with an inner radius, outer radius, and bobbin length of 50 mm, 53 mm, and 100 mm, respectively. The cathode keeper end is placed at the center of the solenoid coil. The axial magnetic field at that location is designated by B.

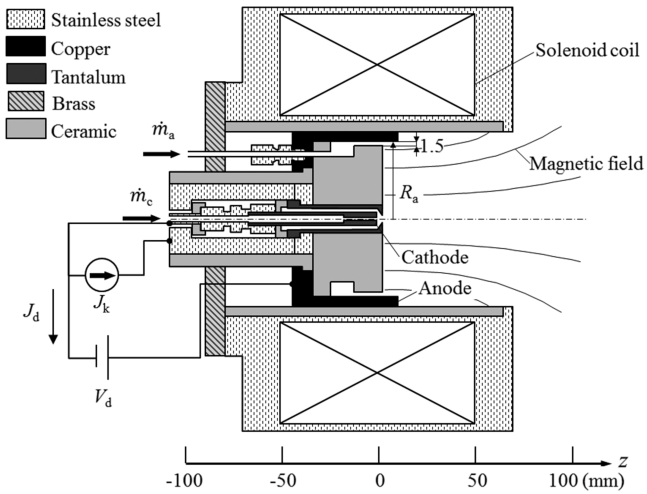

FIG. 1. Schematic of the CC-EST, R_a = 40 mm, side view, length scale in mm.

The basic configuration of the vacuum test facility was unchanged from that reported in Ref. 10. The thruster was mounted on the center axis of a vacuum chamber made of stainless steel, mounted by the pendulum-type thrust stand.[11] The vacuum chamber had a diameter of 2.0 m and a length of 4.0 m. The vacuum pumping system comprised a turbo-molecular pump (3600 L/s, 3203LMC, Shimadzu Co.) backed by a rotary pump (33L/s, 2100D, Alcatel Vacuum Technology). The pendulum arm was supported by two radial ball bearings set on the upper flange on the vacuum chamber. To minimize the radial forces on the bearings, the vertical location of the bearings was adjusted to a balanced position between a gravitational force on the stand, a force due to the difference between atmospheric pressure and the pressure in the vacuum chamber, and an elastic force due to bellows deflection.[11] The deflection of the stand arm was magnified at the tip of a one-meter-long aluminum rod and sensed using a differential transformer.

In this system, the discharge current and the current in the solenoid coil were supplied from outside the vacuum chamber to the pendulum arm using a vacuum feed-through. Between the electromagnetic circuits outside the vacuum chamber and those fixed on the pendulum arm, Lorentz forces were produced and acted as a "tare" force, F_{tare}.[12] To determine the actual thrust produced by the thruster, the tare force had to be corrected. In the present study, F_{tare} was measured by shortening the anode and cathode and varying the current in the discharge circuit, J_{d}, and the current in the solenoid coil, J_{c}, thereby fit to a function of J_{d} and J_{c} of up to the second order. F_{tare} was subtracted from a measured force to obtain a real thrust, F. Among correction terms, a term of CJ_{c} (C, constant), which corresponded to a Lorentz force due to the geomagnetic field exerted on the electric circuit for the coil current, was found dominant. Owing to the geomagnetism, a magnetic field of about 15.9 A/m in the axial direction of the vacuum chamber is exposed inside the vacuum chamber. As the cross section of the solenoid coil was 8800 mm^2, with a magnetic field of 100 mT, the magnetic flux became 1.0×10^{-3} Wb. CJ_{c} was found to be of the order of even 10 mN.

Thrust measurement experiments were conducted with the thruster run using a constant voltage power supply connected to the anode and the cathode. Figure 2(a) shows variations in experimentally measured thrust as a function of the propellant flow rate, $\dot{m}_{\mathrm{a}}$. Under the present experimental conditions, F is almost proportional to $\dot{m}_{\mathrm{a}}$, although it weakly saturates with a large value of $\dot{m}_{\mathrm{a}}$. In an electrostatic thruster, ions are accelerated by an electrostatic force between an available potential drop. The momentum obtained through the electrostatic acceleration equals to the sum of particle momentums. Assuming each particle has a constant exhaust velocity, the thrust is calculated

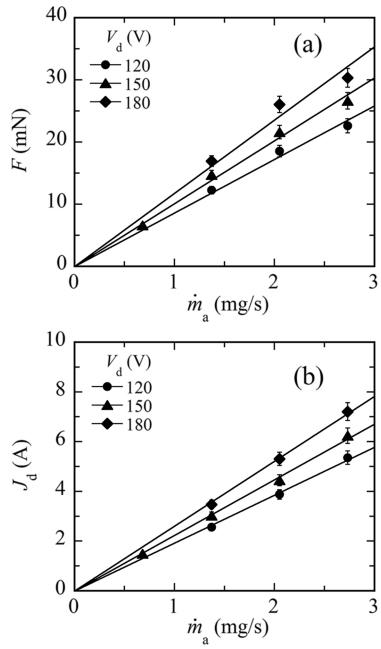

FIG. 2. Thrust and discharge current variations with $\dot{m}_{\mathrm{a}}$, $\dot{m}_{\mathrm{c}}$ = 0.49 mg/s, R_{a} = 40 mm and B = 200 mT.

as the product of the mass flow rate and the exhaust velocity. The thrust variation shown in Fig. 2(a) well fits to this characteristic. Figure 2(b) shows variations in J_d as a function of $\dot{m}_a$. Similar to the thrust variation of Fig. 2(a), J_d increases almost linearly with increasing $\dot{m}_a$, implying that in practice the anode efficiency became almost constant at least within the present operation conditions.

Figure 3(a) shows variations in experimentally measured thrust as a function of the applied magnetic field, B. Under the present operation conditions, F stays not perfectly but almost constant with variation in B. Yet, as shown in Fig. 3(b), J_d decreases with increasing B. This is a typical tendency observed in SPT-type Hall thrusters.[13,14] The stronger the magnetic field, the lower the electron diffusion rate across the magnetic field becomes. In the case of applied-magnetic-field, magneto-plasma-dynamics (MPD) thruster which usually is connected to a constant current power supply, the product of J_dB scales with B because J_d is kept constant. However, in the present operation with a constant voltage power supply, the variation in J_dB with B is suppressed with J_d being decreased. Further discussion will be done in the followings.

As has been shown so far, the thrust and discharge characteristics of the present thruster are well described for electrostatic acceleration. The relationship between thrust and the propellant flow rate in the CC-EST thruster seems to be different from that in the applied-field MPD thrusters,[10,15] in which the thrust is obtained by integrating the Lorentz force, which, in principle, is independent of the propellant mass flow rate. However, it is worth noting that the present thruster exhibited ANOTHER thrust characteristic that cannot be obtained with electrostatic acceleration. It is obvious that the configuration of the present thruster resembles that of an electromagnetic thruster, i.e., an MPD thruster with an applied magnetic field.[16] An important difference between the CC-EST and MPD thrusters is that the thrust in the CC-EST thruster depends on the propellant mass flow rate. However, an electromagnetic thrust in an MPD thruster does not depend on the propellant mass flow rate because the electromagnetic thrust is obtained from the spatial integration of a Lorentz force, which is determined only from the discharge current and magnetic field distributions. Usually an MPD thruster is connected to a constant current power supply. The thrust and discharge voltage are characterized as a function of J_d and B.[17–19] The thrust has an electro-thermal, self-magnetic and electromagnetic components. Tikhonov et al.[17] claimed that an electromagnetic component of $F_{TIK} = C_{TIK}J_dBR_a$ is due to the interaction between an azimuthal Hall current and an applied magnetic field with the coefficient C_{TIK} scaling with a Hall parameter and being evaluated experimentally. Sasoh and Arakawa[18] subdivided an applied-field-oriented thrust into two terms; one is due

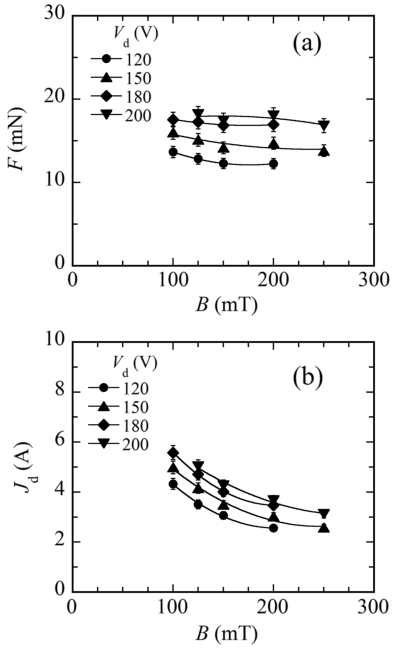

FIG. 3. Thrust and discharge current variations with B, $\dot{m}_c$ = 0.49 mg/s, R_a = 40 mm and $\dot{m}_a$ = 1.37 mg/s.

to the azimuthal Hall current and scales with B^2, and another is due to the swirl motion which is modelled by Fradkin et al.[20] In Fradkin et al.'s "rigid rotator (RR)" model, the plasma is assumed to act as a rigid rotator in the acceleration region, the kinetic energy of the swirl motion is converted to the kinetic energy in the axial direction through the conservations of a total kinetic energy and an angular momentum. They obtained a formula for the thrust, F_{RR}, with even the coefficient being quantified theoretically:

$$F_{\mathrm{RR}} = \frac{1}{\sqrt{2}} \left\{ 1 - \frac{3}{2} \left(\frac{R_{\mathrm{c}}}{R_{\mathrm{a}}} \right)^2 \right\} J_{\mathrm{d}} B R_a \tag{1}$$

where R_{c} is the cathode radius. Again, note here that F_{RR} does not explicitly depend on the mass flow rate of the propellant, $\dot{m}$. Neglecting the second term in the braces, Eq. (1) is approximated to

$$F_{\mathrm{RR}} \cong \frac{1}{\sqrt{2}} J_{\mathrm{d}} B R_a \tag{2}$$

Surprisingly, Eq. (2) agrees well with the experimental performance of the present thruster, as shown in Fig. 4. In this figure, all the experimental data were obtained with various V_{d}, $\dot{m}_{\mathrm{a}}$, B and R_{a}. For $J_{\mathrm{d}} B R_{\mathrm{a}} < 30$ mN, the measured thrust when $R_{\mathrm{a}} = 29$ mm agrees well with the values obtained using Eq. (2). For $J_{\mathrm{d}} B R_{\mathrm{a}} > 30$ mN, in particular when $R_{\mathrm{a}} = 40$ mm, the measured slope in Fig. 4 is slightly smaller than that obtained using Eq. (2). Within a factor greater than 0.75, the measured thrust performance agrees well with the values obtained using Eq. (2), which does not have an explicit dependence on the propellant mass flow rate. The operation runs were conducted by setting the following control parameters of V_{d}, $\dot{m}_{\mathrm{a}}$, B, and R_{a}, whereas the discharge current, J_{d}, was determined passively as a dependent parameter. In the thrust measurement experiments conducted by Ichihara et al.[10] and Albertoni et al.[15] that were done using the applied-field MPD thrusters, $F/(J_{\mathrm{d}} B R_{\mathrm{a}})$ was of the order of 20 % of the coefficient in Eq. (2) or less, whereas in this study, it was 75% to 100%, or even higher. One of large differences between the thrusters is that, in the present study, the propellant is fed only through the narrow slit near the anode, while in the applied-field, MPD thrusters cited above, the propellant was fed through the entire cross-section between the anode and the cathode. In the latter case, the location of propellant ionization is not guaranteed to occur near the anode; the applied electric potential is not necessarily fully utilized for ion acceleration.

Although the thrust generation mechanisms of the present thruster have not been fully understood, we estimate that the thruster operations were conducted under reasonable plasma conditions. Furthermore, the thruster operated under the following conditions: F = 30 mN; $\dot{m}_{\mathrm{a}}$ = 2.75 mg/s; B = 200 mT; V_{d} = 180 V; the exhaust speed, u_{ex}, was estimated to be 1.1×10^4 m/s. Using a representative value $\bar{u} = u_{\mathrm{ex}} / 2$ to estimate a representative plasma density, $\bar{n} = \dot{m}_{\mathrm{a}} / m \bar{u} \pi R_{\mathrm{a}}^2 = 9 \times 10^{17}$ m^{-3} (m, mass of xenon atom). Assuming that both the electrons and ions have an equilibrium temperature of 5 eV, the electron-ion and ion-ion collision frequencies are equal to $\nu_{\mathrm{ei}} = 1.5 \times 10^6$ s^{-1} and $\nu_{\mathrm{ii}} = 1.5 \times 10^3$ s^{-1}, respectively. The travel distances for electron-ion and ion-ion collision are equal to $\bar{u} / \nu_{\mathrm{ei}} = 4 \times 10^{-3}$ m and $\bar{u} / \nu_{\mathrm{ii}} = 2 \times 10^0$ m, respectively. Therefore, in the acceleration region,

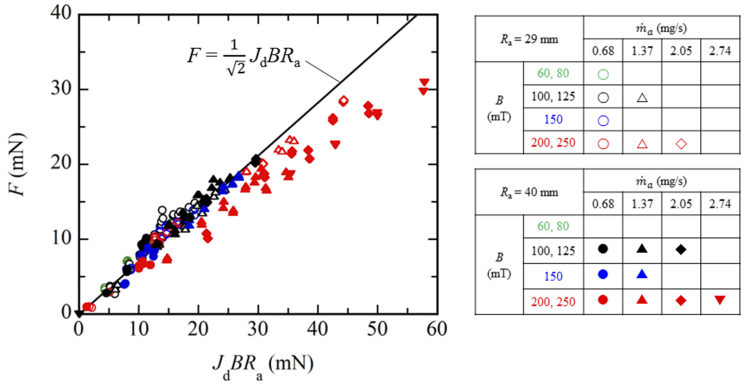

FIG. 4. Thrust characteristics, error in F is ± 5%.

ions do not dissipate their momentum owing to mutual collisions, but gain, with small dissipation, a momentum exerted on the electrons through Hall and diamagnetic effects.

As has been reported so far, this thruster exhibited dual aspects in its thrust performance, i.e., electrostatic and electromagnetic accelerations. Although under the present experimental conditions the thrust almost linearly increased with increasing propellant mass flow rate as for electrostatic acceleration, it also agreed with the thrust performance for swirl acceleration. At present, the mechanisms of these thrust characteristics are still open questions. Moreover, problems such as erosion and life time of thruster components, operation instabilities[21] etc. will be important for practical applications. Therefore, further studies are necessary both experimentally and theoretically.

This work was supported by JSPS KAKENHI(JP15H02321) and by Mitsubishi Heavy Industries Ltd. The authors would like to thank D. Ichihara, J. Jeong and H. Kasuga for their technical assistance in the experiments.

[1] D. M. Goebel and I. Katz, *Fundamentals of Electric Propulsion: Ion and Hall Thrusters*, Chaps. 2 & 7, JPL Space Science and Technology Series, Jet Propulsion Laboratory, California Institute of Technology (2008).
[2] V. Kim, "Main physical features and processes determining the performance of stationary plasma thrusters," J. Prop. Power **14**, 736–743 (1998).
[3] I. G. Mikellides, I. Katz, R. R. Hofer, and D. M. Goebel, "Magnetic shielding of walls from the unmagnetized ion beam in a Hall thruster," Appl. Phys. Lett. **102**, 023509 (2013).
[4] Y. Raitses and N. J. Fisch, "Parametric investigations of a nonconventional Hall thruster," Phys. Plasmas **8**, 2579–2586 (2001).
[5] H. R. Kaufman, R. S. Robinson, and R. I. Seddon, "End-hall ion source," J. Vacuum Sci. & Tech. A **5**, 2081–2084 (1987).
[6] N. Oudini, G. J. M. Hagelaar, J.-P. Boeuf, and L. Garrigues, "Physics and modeling of an end-hall (gridless) ion source," J. Appl. Phys. **109**, 073310 (2011).
[7] S. Harada, T. Baba, A. Uchigashima, S. Yokota, A. Iwakawa, A. Sasoh, T. Yamazaki, and H. Shimizu, "Electrostatic acceleration of helicon plasma using a cusped magnetic field," Appl. Phys. Lett. **105**, 194101 (2014).
[8] A. Uchigashima, T. Baba, D. Ichihara, A. Iwakawa, A. Sasoh, T. Yamazaki, S. Harada, M. Sasahara, and T. Iwasaki, "Anode geometry effects on ion beam energy performance in helicon electrostatic thruster," IEEE Trans. Plasma Sci. **44**, 306–313 (2016).
[9] D. Ichihara, A. Uchigashima, A. Iwakawa, and A. Sasoh, "Electrostatic ion acceleration across a diverging magnetic field," Appl. Phys. Lett. **109**, 053901 (2016).
[10] D. Ichihara, T. Uno, H. Kataoka, J. Jeong, A. Iwakawa, and A. Sasoh, "Ten-ampere-level, applied-field-dominant operation in magnetoplasmadynamic thrusters," J. Propuls. Power **33**, 360–369 (2017).
[11] A. Sasoh and Y. Arakawa, "A high-resolution thrust stand for ground tests of low-thrust space propulsion devices," Rev. Sci. Instrum. **64**, 719–723 (1993).
[12] A. Sasoh and Y. Arakawa, "Electromagnetic effects in an applied-field magnetoplasmadynamic thruster," J. Prop. Power **8**, 98–102 (1992).
[13] J. M. Sankovic, J. A. Hamley, and T. W. Haag, Performance Evaluation of the Russian SPT Thruster at NASA LeRC in Proceedings of the 23th International Electric propulsion Conference, IEPC Paper No. 1993-094, Seattle, Washington, USA, 1993.
[14] D. Manzella, C. Sarmiento, J. Sankovic, and T. Haag, Performance Evaluation of the SPT-140 in Proceedings of the 25th International Electric propulsion Conference, IEPC Paper No. 1997-059, Cleveland, Ohio, USA, 1997.
[15] R. Albertoni, F. Paganucci, P. Rossetti, and M. Andrenucci, "Experimental study of a hundred-kilowatt-class applied-field magnetoplasmadynamic thruster," J. Prop. & Power **29**, 1138–1145 (2013).
[16] G. Krulle, M. A. Kurtz, and A. Sasoh, "Technology and application aspects of applied field magnetoplasmadynamic propulsion," J. Prop. Power **14**, 754–763 (1998).
[17] V. B. Tikhonov, S. A. Semenikhin, J. R. Brophy, and J. E. Polk, Performance of 130 kw MPD Thruster with an External Magnetic Field and Li as a Propellant in Proceedings of the 25th International Electric Propulsion Conference, IEPC Paper No. 97-117, Cleveland, Ohio, USA, 1997.
[18] A. Sasoh and Y. Arakawa, "Thrust formula for applied-field magnetoplasmadynamic thrusters derived from energy conservation equation," J. Prop. & Power **11**, 351–356 (1995).
[19] R. M. Myers, "Geometric scaling of applied-field magnetoplasmadynamic thrusters," J. Prop. & Power **11**, 343–350 (1995).
[20] D. B. Fradkin, A. W. Blackstock, D. J. Roehling, T. F. Stratton, M. Williams, and K. W. Liewer, "Experiments using a 25-kw hollow cathode lithium vapor mpd arcjet," AIAA J. **8**, 886–894 (1970).
[21] H. K. Malik and S. Singh, "Resistive instability in a Hall plasma discharge under ionization effect," Phys. Plasmas **20**, 052115 (2013).